Crystal structures and magnetic properties of novel rare-earth copper sulfides, $EuRCuS_3$ (R = Y, Gd–Lu)

2004 J. Phys.: Condens. Matter 16 5503

(http://iopscience.iop.org/0953-8984/16/30/012)

INSTITUTE OF PHYSICS PUBLISHING JOURNAL OF PHYSICS: CONDENSED MATTER

J. Phys.: Condens. Matter **16** (2004) 5503–5518 PII: S0953-8984(04)79766-0

Crystal structures and magnetic properties of novel rare-earth copper sulfides, $EuRCuS_3$ (R = Y, Gd–Lu)

Makoto Wakeshima, Fumito Furuuchi and Yukio Hinatsu

Division of Chemistry, Graduate School of Science, Hokkaido University, Sapporo 060-0810, Japan

Received 22 April 2004
Published 16 July 2004
Online at stacks.iop.org/JPhysCM/16/5503
doi:10.1088/0953-8984/16/30/012

Abstract

Novel quaternary rare-earth copper sulfides $EuRCuS_3$ (R = Y, Gd–Lu excluding Ho, Er) have been investigated by means of x-ray diffraction, magnetic susceptibility, magnetization, and specific heat measurements. These compounds crystallize in the Eu_2CuS_3-type structure for R = Y, Gd–Dy and in the $KZrCuS_3$-type structure for R = Tm–Lu. Both $EuYCuS_3$ and $EuLuCuS_3$ show a ferromagnetic transition and the other $EuRCuS_3$ compounds show a ferrimagnetic transition at around 5.0 K.

1. Introduction

Ternary and quaternary copper sulfides containing rare-earth ions frequently crystallize in low dimensional structures and display interesting physical properties [1]. Ternary europium copper sulfide Eu_2CuS_3 has been reported to crystallize in the orthorhombic structure with space group *Pnma* [2]. The schematic structure of Eu_2CuS_3 is illustrated in figure 1(a). In this structure, the Eu ions occupy two crystallographically independent sites. The Eu(1) ion is coordinated by six sulfur ions and the $Eu(1)S_6$ octahedra share corners along the *a*-axis and edges along the *b*-axis. The Eu(1) S_6 octahedra and CuS_4 tetrahedra form a $CuEu(1)S_3$ layer perpendicular to the *c*-axis. The Eu(2) ions are coordinated by seven sulfur ions between the $CuEu(1)S_3$ layers, forming $Eu(2)S_7$ monocapped trigonal prisms. This compound has the formal oxidation state $Eu^{2+}Eu^{3+}Cu^{+}S_3^{2-}$ and the Eu^{2+} and Eu^{3+} ions are supposed to occupy the Eu(2) and Eu(1) sites, respectively, from the Eu–S distances [2].

Recently, we have carried out magnetic susceptibility, specific heat, and ^{151}Eu Mössbauer spectroscopy measurements for Eu_2CuS_3 [3]. Its ^{151}Eu Mössbauer spectra reveal that the Eu^{2+} and Eu^{3+} ions occupy the Eu(2) and Eu(1) sites independently below room temperature. Furthermore, Eu_2CuS_3 shows a ferromagnetic transition at 3.4 K due to magnetic interactions among the Eu^{2+} ions with the $^8S_{7/2}$ ground state.

Because the Eu^{3+} ion has a non-magnetic ground state ($^7F_0$), its magnetic contribution to the magnetic behaviour of Eu_2CuS_3 is negligible at low temperatures. In order to investigate

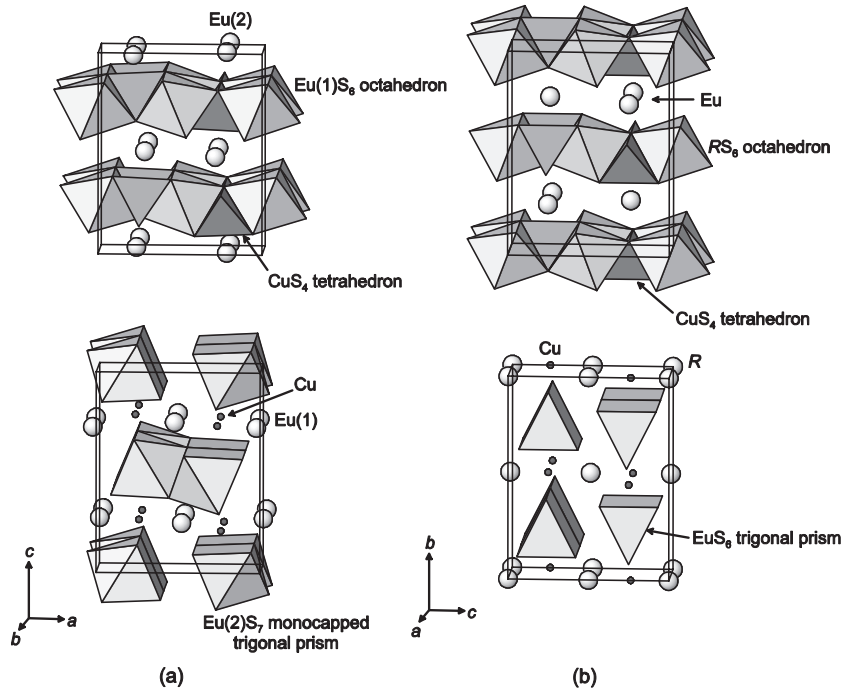

Figure 1. Polyhedral representations of the Eu_2CuS_3-type (a) and $KZrCuS_3$-type (b) structures.

the magnetic behaviour of trivalent rare-earth ions other than the Eu^{3+} ion, we have attempted to synthesize new quaternary rare-earth copper sulfides $EuRCuS_3$ (R = rare earths) in which half of the Eu sites in the Eu_2CuS_3 are replaced by rare-earth ions. In this paper, we will report the results of the magnetic susceptibility, magnetization, and specific heat measurements of $EuRCuS_3$.

2. Experimental details

Quaternary rare-earth copper sulfides, $EuRCuS_3$, were synthesized by a solid-state reaction. Rare-earth sesquioxide (R_2O_3) and copper oxide (CuO) were used as starting materials. The stoichiometric mixture of the starting materials was heated in a graphite boat at 1170–1320 K in a flow of mixed CS_2 and N_2 gas which was obtained by bubbling the N_2 gas through liquid CS_2 at room temperature. The reaction was carried out at the same temperature for 18–36 h, with several intervals of regrinding.

Powder x-ray diffraction measurements were performed with Cu Kα radiation on a Rigaku MultiFlex diffractometer equipped with a curved graphite monochromator. Intensity data were collected by step scanning in the range 10°–120° at intervals of 0.02°. The structure and lattice parameters were refined with a Rietveld program, RIETAN 2000 [4].

Magnetic susceptibility measurements were performed with a SQUID magnetometer (Quantum Design MPMS model) from 1.8 to 300 K. Susceptibility versus temperature curves for each sample were measured under both the ZFC (zero-field-cooled) and FC (field-cooled) conditions. The former were measured on heating the sample to 300 K after zero-field cooling to 1.8 K, applying a field of 0.1 T. The latter were measured on cooling from 300 to 1.8 K at 0.1 T. Additionally, around the magnetic transition temperatures, the magnetic susceptibility measurements were also performed in the much smaller magnetic field of 5 mT. The field

Table 1. Lattice parameters and R factors of $EuRCuS_3$. (Note: $R_{wp} = [\sum_i w_i(y_i - f_i(x))^2 / \sum_i w_i y_i^2]^{1/2}$ and $R_I = \sum |I_k(o) - I_k(c)| / \sum I_k(o)$.)

R	Type	a (Å)	b (Å)	c (Å)	R_{wp} (%)	R_I (%)
Y	Eu_2CuS_3	10.1830(3)	3.9260(1)	12.8482(4)	6.84	2.20
Eu	Eu_2CuS_3	10.3619(3)	3.9596(1)	12.9224(4)	7.90	2.59
Gd	Eu_2CuS_3	10.3187(3)	3.9487(1)	12.8319(4)	7.35	1.94
Tb	Eu_2CuS_3	10.2495(3)	3.9366(1)	12.8362(4)	6.86	2.32
Dy	Eu_2CuS_3	10.1904(3)	3.9267(1)	12.8471(4)	7.20	1.80
Tm	$KZrCuS_3$	3.9042(1)	12.8498(3)	10.0401(2)	6.86	2.19
Yb	$KZrCuS_3$	3.8965(1)	12.8451(3)	10.0028(2)	7.30	2.28
Lu	$KZrCuS_3$	3.8915(1)	12.8470(3)	9.9840(2)	8.68	2.73

dependence of the magnetization was measured at 1.8–10 K by changing the applied magnetic field between 0 and 5 T.

The specific heat measurement was carried out using a relaxation technique supplied by commercial specific heat measurement system equipped with the ^{3}He option (Quantum Design, PPMS) in the temperature range from 0.4 to 300 K. The sample in the form of a pellet (∼10 mg) was mounted on an aluminium plate with apiezon grease for better thermal contact.

3. Results and discussion

3.1. Crystal structure

The $EuRCuS_3$ (R = Y, Sm–Lu) phase was identified from the x-ray diffraction (XRD) profiles. However, the samples for R = Sm, Ho and Er contain more than 3 wt% of $(Eu, R)_2O_2S$ as an impurity. Attempts to synthesize the Nd compound were unsuccessful and led to multiphasic samples without the $EuNdCuS_3$ phase. Figures 2(a) and (b) show the XRD profiles for $EuDyCuS_3$ and $EuTmCuS_3$, respectively. The profile for $EuDyCuS_3$ is indexed with respect to an orthorhombic Eu_2CuS_3-type cell with the space group $Pnma$, while the hkl reflections with odd $(h + l)$ disappear in the profile of $EuTmCuS_3$. The Yb and Lu compounds also show similar XRD profiles to $EuTmCuS_3$. These results indicate that the $EuRCuS_3$ compounds containing small R ions (R = Tm, Yb, Lu) crystallize in the B base-centred lattice. The $BaRMQ_3$ (R = rare earths; M = Cu, Ag, Au; Q = S, Se, Te) compounds transform from the Eu_2CuS_3-type structure (space group $Pnma$) to the $KZrCuS_3$-type structure (space group $Cmcm$) depending on the size of the R ion [5–7]. The space group, $Bbmm(Cmcm)$, for the B base-centred cell is a supergroup of $Pnma$, and all the Bragg reflections for the $EuRCuS_3$ compounds with R = Tm, Yb, Lu are indexed with respect to the orthorhombic $KZrCuS_3$-type cell with the space group $Cmcm$. For all the $EuRCuS_3$ compounds except for those with R = Sm, Ho, and Er, the crystallographic parameters were refined by the Rietveld method. The calculated XRD profiles are in good agreement with the observed ones ($R_{wp} = 7.20\%$, $R_I = 1.80\%$ for $EuDyCuS_3$ and $R_{wp} = 6.86\%$, $R_I = 2.19\%$ for $EuTmCuS_3$) as shown in figure 2. The lattice parameters and the positional parameters are listed in tables 1 and 2, respectively.

Figure 1(b) illustrates the crystal structure of $KZrCuS_3$-type $EuRCuS_3$. The schematic features of the $KZrCuS_3$-type structure are similar to those of the Eu_2CuS_3-type structure. The distorted RS_6 octahedra share edges along the b-axis and share corners along the c-axis, forming two-dimensional sheets in the b–c plane. The CuS_4 tetrahedra share corners along the c-axis and share their edges with the RS_6 octahedra. However, each Eu ion is coordinated

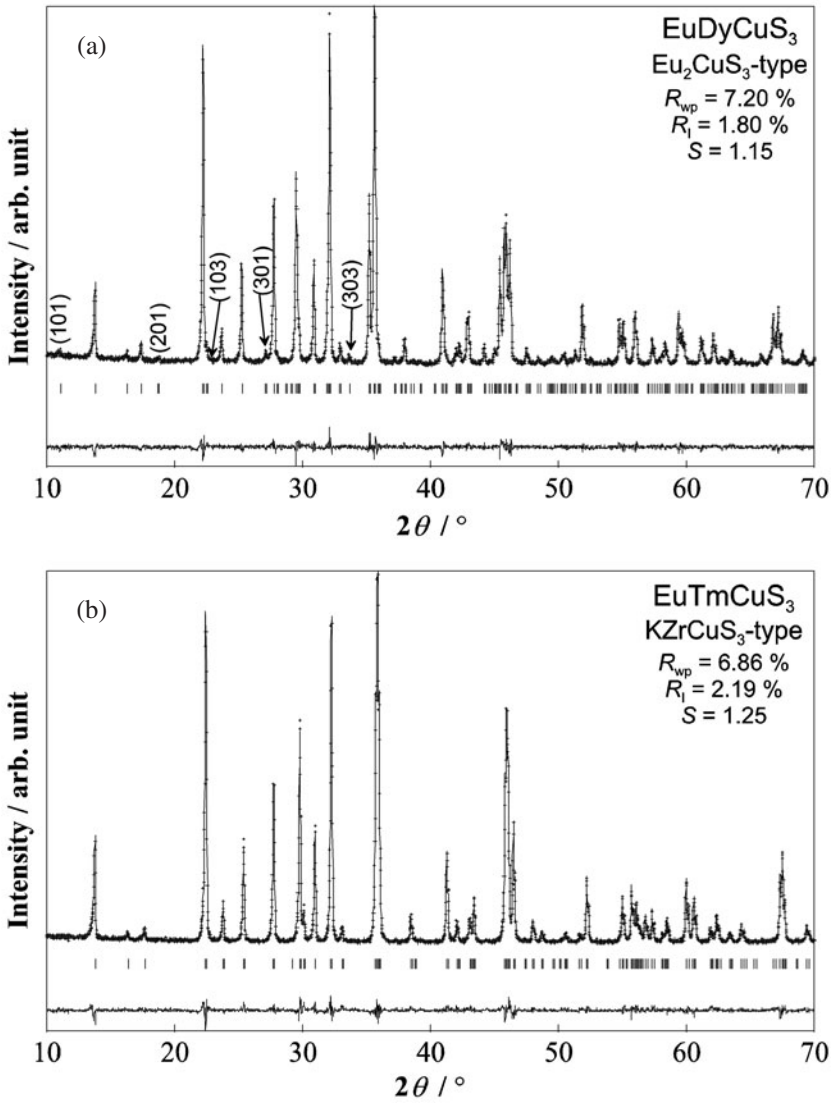

Figure 2. Powder x-ray diffraction patterns and Rietveld refinements for $EuDyCuS_3$ (a) and $EuTmCuS_3$ (b). The bottom trace is a plot of the difference between the observed (cross markers) and calculated (solid curve) intensities. All allowed Bragg reflections are shown by vertical lines.

by six sulfur atoms and the EuS_6 prisms share faces, forming one-dimensional chains along the c-axis, while each Eu(2) ion in the Eu_2CuS_3-type structure is coordinated by seven sulfur ions, forming $Eu(2)S_7$ monocapped trigonal prisms.

Figure 3 shows the difference, $\Delta/\% = \frac{l(\mathrm{R})-l(\mathrm{Eu})}{l(\mathrm{Eu})} \times 100$ (l(R) is the lattice parameter of $EuRCuS_3$), between the lattice parameters of Eu_2CuS_3 ($a = 10.3602(3)$ Å, $b = 3.9589(1)$ Å, $c = 12.8202(3)$ Å) and $EuRCuS_3$ against the ionic radius of the six-coordinated R^{3+} ion. The lattice parameters, a_{Cmcm}, b_{Cmcm}, and c_{Cmcm}, for the $KZrCuS_3$-type structure correspond to b_{Pnma}, c_{Pnma}, and a_{Pnma} for the Eu_2CuS_3-type structure, respectively. No discontinuous change of lattice parameters with the R^{3+} ionic radius is observed, although the symmetry of

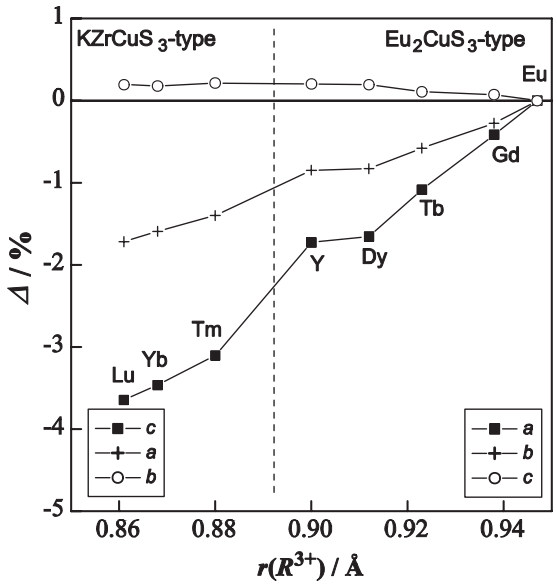

Figure 3. The difference, Δ (%), in lattice parameters between Eu_2CuS_3 and $EuRCuS_3$ against the ionic radius of the six-coordinated R^{3+} ion (see the text).

Table 2. Positional parameters for $EuDyCuS_3$ and $EuTmCuS_3$.

	Site	x	y	z	B (Å^2)
		$EuDyCuS_3$	SG: *Pnma*		
Eu	4c	0.7713(2)	1/4	0.0018(1)	0.74(8)
Dy	4c	0.0129(2)	1/4	0.7423(1)	0.52(8)
Cu	4c	0.2378(4)	1/4	0.2224(2)	1.06(10)
S(1)	4c	0.0511(6)	1/4	0.1140(5)	0.51(17)
S(2)	4c	0.4146(6)	1/4	0.1074(5)	0.44(17)
S(3)	4c	0.2607(7)	1/4	0.8278(4)	0.42(15)
		$EuTmCuS_3$	SG: *Cmcm*		
Eu	4c	0	0.7480(1)	1/4	0.97(8)
Tm	4a	0	0	0	0.35(7)
Cu	4c	0	0.4711(1)	1/4	1.02(9)
S(1)	8f	0	0.3612(3)	0.0669(3)	0.66(10)
S(2)	4c	0	0.0779(4)	1/4	0.85(14)

the crystal structures changes between the Y and Tm compounds. With decreasing R^{3+} ionic radius, a_{Pnma} (c_{Cmcm}) and b_{Pnma} (a_{Cmcm}) decrease, but c_{Pnma} (b_{Cmcm}) increases slightly. This tendency has also been observed in the lattice parameters for other isomorphic compounds, $BaRMQ_3$ (M = Cu, Ag, Au; Q = S, Se, Te) and $CsRMSe_3$ (M = Zn, Cd, Hg) [5–7].

Selected interatomic distances between cation and sulfide ions are plotted in figure 4. The coordination polyhedra of the R ions in the Eu_2CuS_3-type and $KZrCuS_3$-type structures are similar, with six sulfur neighbours forming distorted octahedra. The Cu ions have four sulfur neighbours forming distorted tetrahedra in both the Eu_2CuS_3-type and $KZrCuS_3$-type structures. The R–S distances decrease monotonically with decreasing R^{3+} ionic radius, while the Cu–S distances are almost constant (2.32–2.40 Å). On the other hand, the Eu–S interatomic distances show a discontinuous change between the Y and Tm compounds, which is due to the transformation from the Eu_2CuS_3-type to the $KZrCuS_3$-type structure. Sulfur coordinations

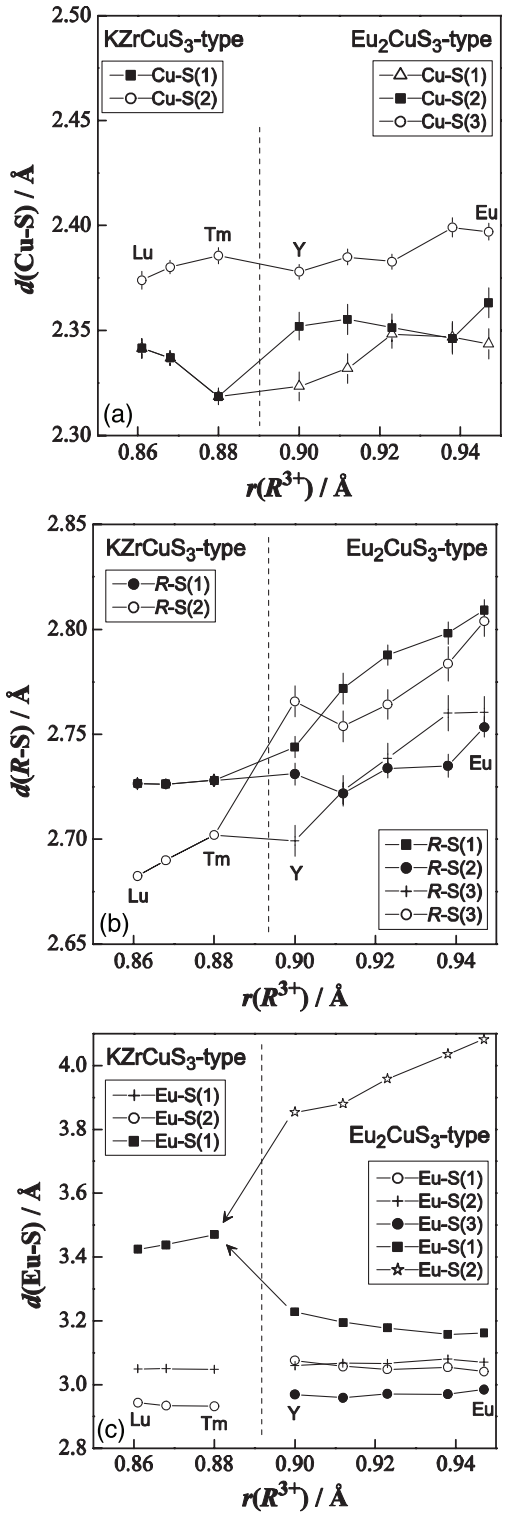

Figure 4. Interatomic distances, d(Cu–S), d(R–S), and d(Eu–S), for $EuRCuS_3$.

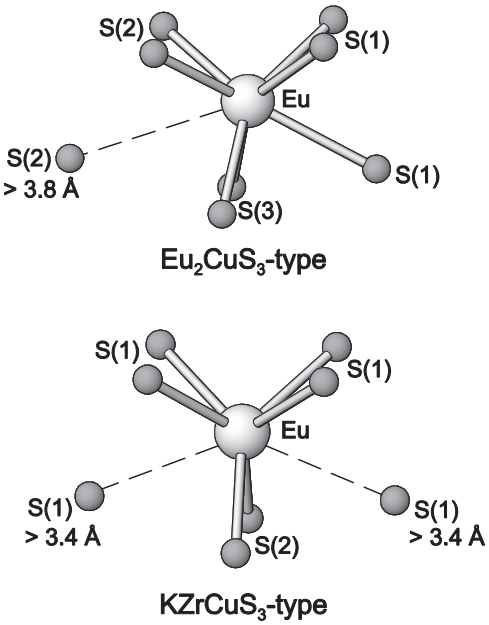

Figure 5. The coordination of the Eu^{2+} ion in the Eu_2CuS_3-type and $KZrCuS_3$-type structures.

around the Eu ion in the $EuRCuS_3$ compounds are illustrated in figure 5. For the Eu_2CuS_3-type structure, seven Eu–S distances (Eu–S(1) × 1, Eu–S(1) × 2, Eu–S(2) × 2, and Eu–S(3) × 2) are shorter than 3.2 Å, but one Eu–S(2) distance is remarkably long (>3.8 Å). With decreasing R^{3+} ionic radius, one Eu–S(1) distance gradually becomes long, and it shows a discontinuous increase between the Y and Tm compounds. Consequently, in the $KZrCuS_3$-type structure, the Eu ions have six closer sulfur neighbours (Eu–S(1) × 4, Eu–S(2) × 2) and two additional S(1) ions (>3.4 Å). The eighth sulfide ion in the Eu_2CuS_3-type structure and the seventh (eighth) sulfide ions in the $KZrCuS_3$-type structure can only marginally be counted as neighbours of the Eu ions.

3.2. Magnetic property

3.2.1. $EuYCuS_3$ and $EuLuCuS_3$. The insets of figures 6(a) and (b) show the reciprocal magnetic susceptibilities (χ^{-1}) of $EuYCuS_3$ and $EuLuCuS_3$ as a function of temperature in the magnetic field of 0.1 T. Only the Eu^{2+} ion is magnetic in these compounds. Thus, the molar susceptibility is given by

$$\chi = \chi(\mathrm{Eu}^{2+}) + \chi_{\mathrm{TIP}}, \tag{1}$$

where χ_{TIP} is the temperature-independent term containing the diamagnetic term. For the ground $^8S_{7/2}$ state of the Eu^{2+} ion, the orbital angular momentum vanishes, and so the crystal field does not affect the susceptibility of the Eu^{2+} ion. Consequently, the magnetic susceptibility of Eu^{2+} is represented by $N_{\mathrm{A}}\mu_{\mathrm{eff}}(\mathrm{Eu}^{2+})^2/3k_{\mathrm{B}}(T-\Theta_{\mathrm{W}})$, where k_{B} is Boltzmann's constant and μ_{eff} is the effective magnetic moment. The values of μ_{eff} and Θ_{W} for Eu^{2+} were determined as 7.77(3) μ_{B} and +7.1(1) K for $EuYCuS_3$, and 7.82 μ_{B} and +6.1 K for $EuLuCuS_3$, respectively. The effective magnetic moment is in good agreement with the theoretical one ($g\sqrt{S(S+1)} = 7.94\ \mu_{\mathrm{B}}$). The positive sign of Θ_{W} is indicative of a ferromagnetic coupling between the Eu^{2+} ions in $EuYCuS_3$ and $EuLuCuS_3$. Figures 6(a) and (b) show the magnetic susceptibility below 10 K for $EuYCuS_3$ and $EuLuCuS_3$, respectively. A divergence between

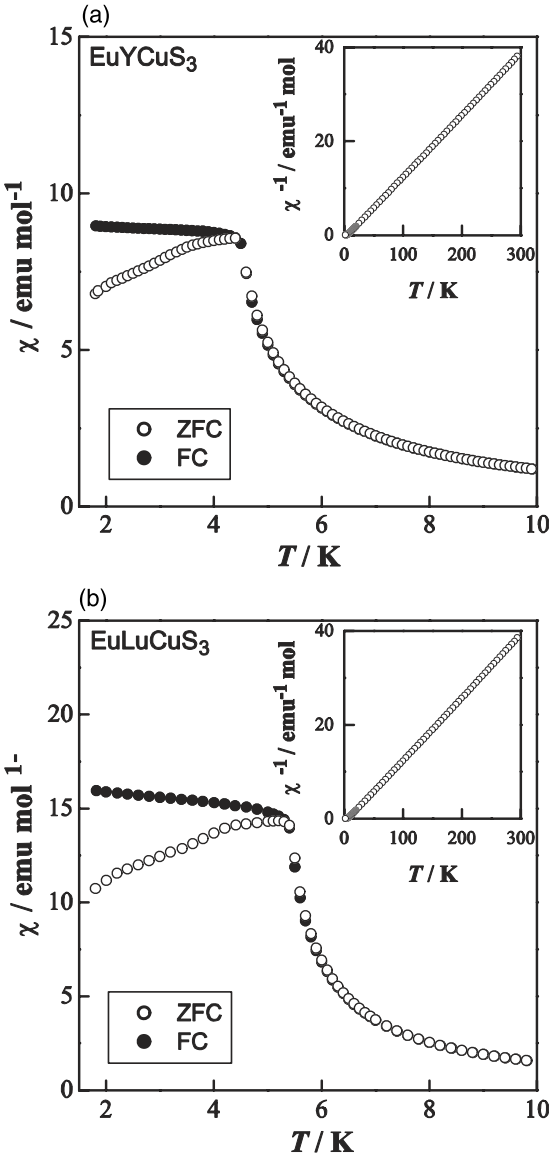

Figure 6. The temperature dependence of the magnetic susceptibility (χ) for $EuYCuS_3$ (a) and $EuLuCuS_3$ (b) below 10 K. The insets show the reciprocal magnetic susceptibility (χ^{-1}) below 300 K.

the ZFC and FC susceptibilities, which is due to the ferromagnetic transition, has been observed at 4.5 K for $EuYCuS_3$ and at 5.4 K for $EuLuCuS_3$.

Figures 7(a) and (b) show the field dependence of the magnetization (M) below and above the Curie temperature for $EuYCuS_3$ and $EuLuCuS_3$, respectively. For both compounds, the magnetization at 2 K (below the Curie temperature) increases linearly with the applied field and almost saturates at 1.5 T. The features of these M–H curves are suggestive of a soft ferromagnet with very small hysteresis. Extrapolation of the high field magnetic moment to zero field yielded a saturation moment of 6.8 μ_B for $EuYCuS_3$ and 6.6 μ_B for $EuLuCuS_3$. These values agree with the theoretical value of $gS = 7\ \mu_B$ for the ferromagnetic ordering of the Eu^{2+} ion which is in the $^8S_{7/2}$ state. The magnetization curves at 10 K (above the Curie temperature) can be scaled by the Brillouin function $M = gSB_S(x)$ with $S = 7/2$ ($x = gS\ \mu_B H/k_B T^*$)

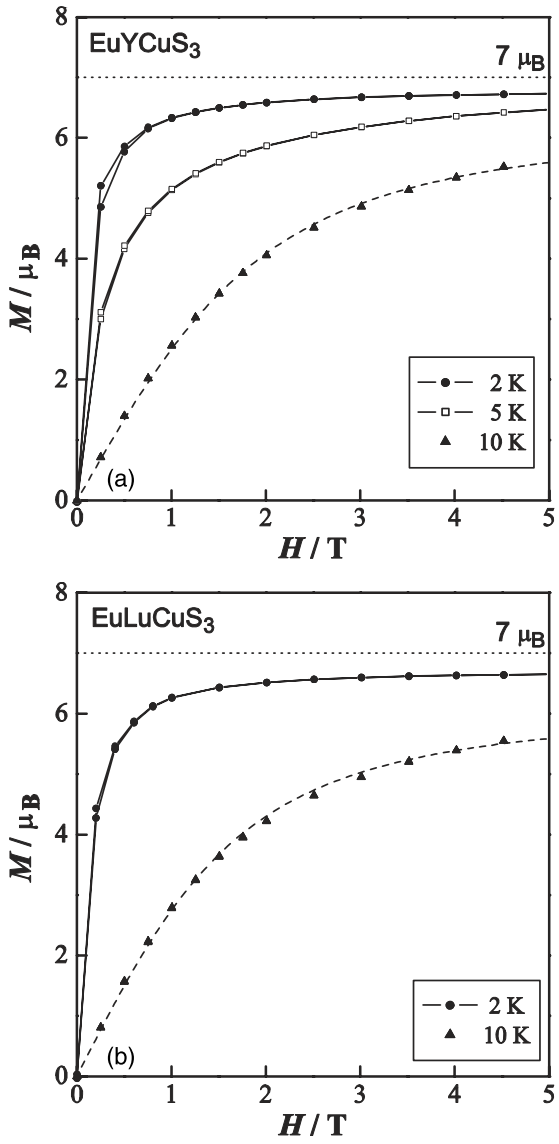

Figure 7. The field dependence of the magnetization for $EuYCuS_3$ (a) and $EuLuCuS_3$ (b). Broken lines are the results of fitting with the Brillouin function $M = gSB_S(x)$ (see the text).

modified by the effective temperature $T^* = T - \Theta_W$, which is plotted as the broken line in figure 7. The Curie–Weiss temperatures (Θ_W) are estimated to be +5.5 K for $EuYCuS_3$ and +6.1 K for $EuLuCuS_3$. These temperatures are comparable to those derived from the Curie–Weiss fitting to the χ^{-1}–T curve.

The specific heat (C_p) of $EuYCuS_3$ was measured in the temperature range from 0.4 to 300 K as shown in the inset of figure 8(a). The sharp λ-type anomaly at 4.4 K is indicative of a long range magnetic ordering which corresponds to the ferromagnetic transition observed in the χ–T and M–H curves (see figures 6, 7). The specific heat of insulating $EuYCuS_3$ consists of a lattice contribution (C_{lat}) and a magnetic contribution (C_{mag}). C_{lat} is represented by the usual harmonic lattice series in odd powers of temperature T:

$$C_{lat} = B_3T^3 + B_5T^5 + B_7T^7 + \cdots. \tag{2}$$

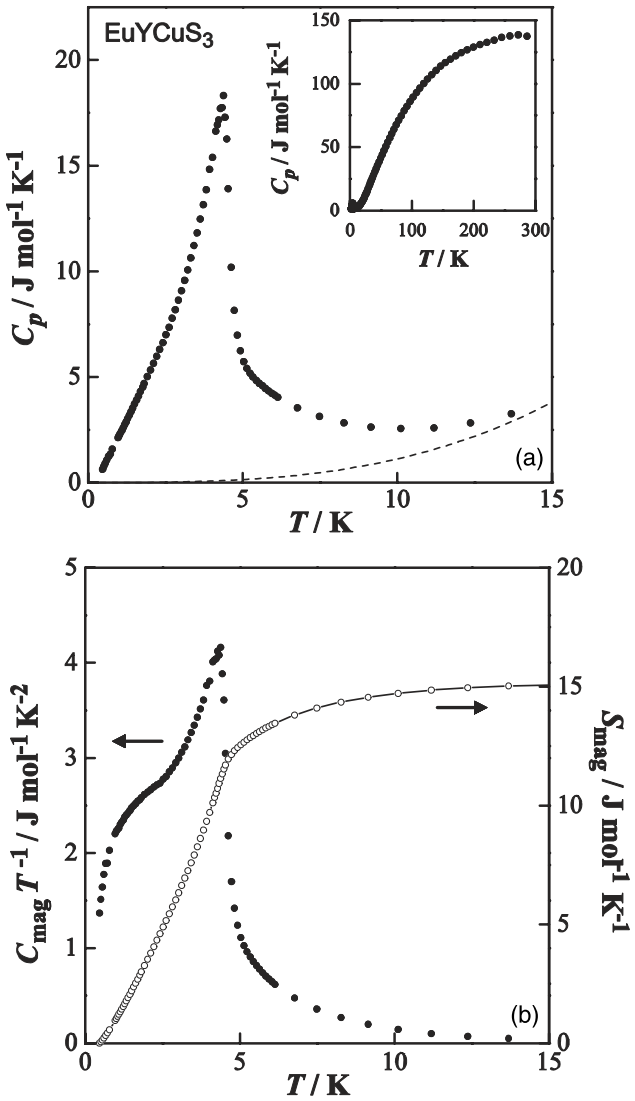

Figure 8. (a) The temperature dependence of the specific heat (C_p) below 15 K for $EuYCuS_3$. The inset shows the specific heat behaviour up to 300 K. (b) The temperature dependence of the magnetic specific heat (C_{mag}/T) divided by the temperature and magnetic entropy (S_{mag}) below 15 K for $EuYCuS_3$.

On the assumption that C_{mag} is negligible above 16 K, the constants B_3, B_5, B_7 were determined by fitting equation (2) to the observed specific heat data between 16 and 25 K. C_{mag} is obtained by subtracting C_{lat} from the total C_p. The temperature dependences of C_{mag}/T and the magnetic entropy calculated from $S_{mag} = \int (C_{mag}/T)\,dT$ are shown in figure 8(b). From the S_{mag}–T curve, the magnetic entropy change is estimated to be $\sim$15 J mol^{-1} K^{-1}, and it is close to $R\ln(2S+1) = R\ln 8$ (17.3 J mol^{-1} K^{-1}). This result reveals that the ferromagnetic ordering of $EuYCuS_3$ is caused by only the Eu^{2+} ion and the eightfold degeneracy remains in the ground state of Eu^{2+}, which is consistent with the results obtained through the magnetic susceptibility and magnetization measurements.

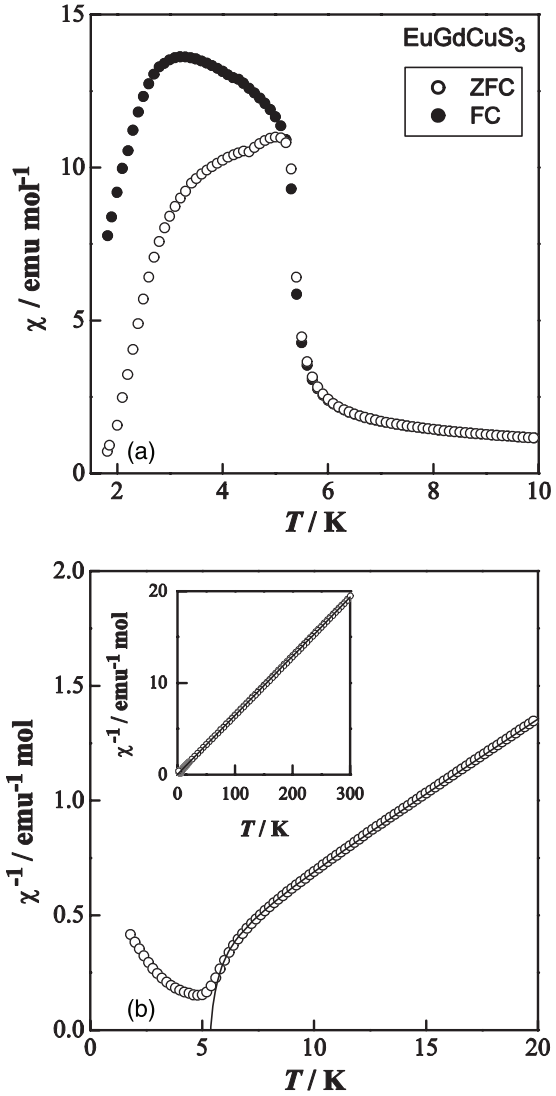

Figure 9. (a) The temperature dependence of the magnetic susceptibility (χ) for $EuGdCuS_3$ below 10 K. (b) The temperature dependence of the reciprocal magnetic susceptibility (χ^{-1}) for $EuGdCuS_3$ below 20 K. The inset shows the reciprocal magnetic susceptibility (χ^{-1}) below 300 K. A solid curve is the result of fitting with the molecular field approximation (see the text).

3.2.2. $EuGdCuS_3$. Figure 9(a) shows the temperature dependence of the magnetic susceptibilities χ below 10 K. With decreasing temperature, χ increases abruptly at 5.6 K and the ZFC susceptibility diverges from the FC susceptibility below 5.2 K. The ZFC susceptibility decreases gradually below 5.2 K and shows an abrupt drop below 3.0 K. On the other hand, the FC susceptibility still increases below 5.2 K and then decreases abruptly below 3.0 K.

The reciprocal magnetic susceptibility (χ^{-1}) versus temperature curve for $EuGdCuS_3$ is shown in the inset of figure 9(b). In this compound, since both the Eu^{2+} and Gd^{3+} ions have the $^8S_{7/2}$ ground state without orbital momentum, the crystal electric field does not affect the magnetic susceptibility. Therefore, it is expected that the molar susceptibility can be

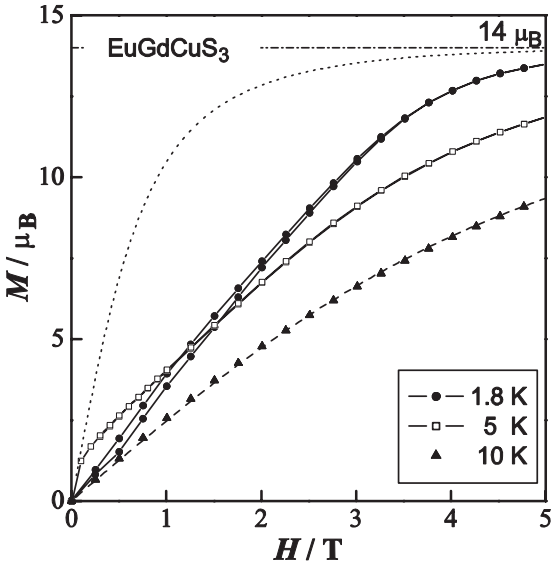

Figure 10. The field dependence of the magnetization for $EuGdCuS_3$. The broken and dotted curves represent the Brillouin function $M = gSB_S(x)$ with $\Theta_W = -1.2$ K at 10 K and with $\Theta_W = 0$ K at 1.8 K, respectively (see the text).

represented as

$$\chi = \chi(Eu^{2+}) + \chi(Gd^{3+}) + \chi_{TIP} = \frac{C}{T - \Theta_W} + \chi_{TIP}. \tag{3}$$

From the Curie–Weiss law fitting to the χ^{-1}–T curves in the temperature range between 10 and 300 K, C and Θ_W are estimated to be 15.5(3) emu K mol^{-1} and $-0.72(1)$ K, respectively. This Curie constant agrees with the theoretical one (15.8 emu K mol^{-1}), but the Curie–Weiss temperature is very small as compared with the magnetic anomaly temperature in the χ–T curve.

The field dependence of the magnetization for $EuGdCuS_3$ is shown in figure 10. The M–H curve at 10 K (in the paramagnetic region) can be scaled by the Brillouin function $M = 2gSB_S(x)$ with $S = 7/2$ and $\Theta_W = -1.2$ K (a broken line). This Curie–Weiss temperature is close to that ($\Theta_W = -0.72$ K) obtained by the Curie–Weiss fitting. Below the magnetic anomaly temperature (5.6 K), the M–H curve shows complicated behaviour. In the M–H curve at 5 K, M reaches 1.2 μ_B at 100 mT, but increases gradually above 100 mT. On the other hand, M at 1.8 K increases gently with the applied field compared with the theoretical curve $M = 2gSB_S(x)$ with $\Theta_W = 0$ K at 1.8 K (a dotted curve in figure 10). Therefore the M–H curve at 5.0 K suggests that the magnetic ordering state at 5.0 K is ferrimagnetic, while the M–H curve at 1.8 K is indicative of antiferromagnetic couplings between the Gd^{3+} and Eu^{2+} moments.

The temperature dependences of C_{mag}/T and S_{mag} for $EuGdCuS_3$ were derived in a similar manner to those for $EuYCuS_3$, and they are shown in figure 11. The λ-type anomaly at 5.1 K in the C_{mag}/T–T curve suggests that a long range magnetic ordering occurs at this temperature. Below 5.1 K, the features of C_{mag}/T for $EuGdCuS_3$, which has a broad maximum at around 1.5 K, are different from those for $EuYCuS_3$. The change of S_{mag} approaches $\sim 2R \ln 8$ (34.6 J mol^{-1} K^{-1}) at 15 K, which indicates that the Eu^{2+} and Gd^{3+} ions have the same $^8S_{7/2}$ ground state and contribute to the magnetic ordering of $EuGdCuS_3$.

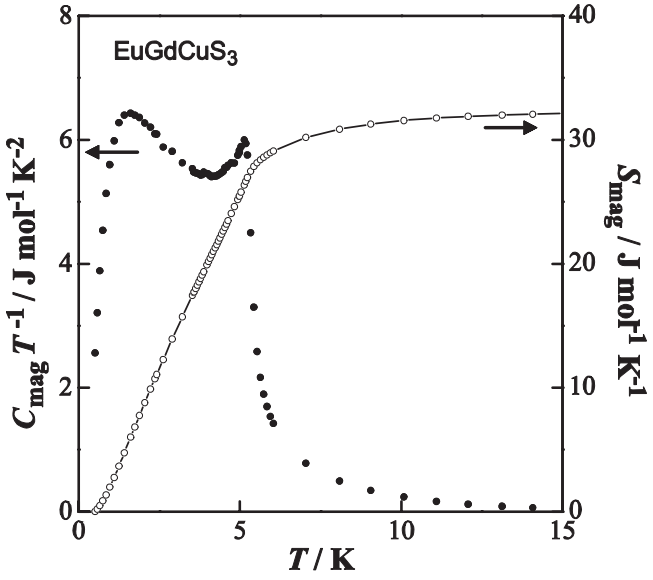

Figure 11. The temperature dependence of the magnetic specific heat (C_{mag}/T) divided by the temperature and magnetic entropy (S_{mag}) below 15 K for $EuGdCuS_3$.

For $EuRCuS_3$ (R = Y, Eu, Lu) containing non-magnetic R ions, the ferromagnetic ordering of the Eu^{2+} moments occurs at 3.4–4.4 K, while the $EuRCuS_4$ (R = Tb–Yb) compounds containing magnetic R ions show ferrimagnetic behaviour as will be described later. Thus, it is considered that each of the Eu^{2+} and Gd^{3+} moments ($S = 7/2$) forms a ferromagnetic net and that the antiferromagnetic interaction operates between the Eu^{2+} and Gd^{3+} ferromagnetic nets. The difference in ordered magnetic moment between the Eu^{2+} and Gd^{3+} ferromagnetic nets causes the divergence between the ZFC and FC susceptibilities below 5.2 K (figure 9(a)) and the ferrimagnetic M–H curve at 5 K (figure 10). At even lower temperatures, the ordered magnetic moments of the Eu^{2+} and Gd^{3+} ions should both approach 7 μ_B, and it is supposed that the drops of the ZFC and FC susceptibilities below 3.0 K and the M–H curve at 1.8 K are due to the antiferromagnetic coupling between the Eu^{2+} and Gd^{3+} ferromagnetic nets with the same ordered moments. In view of these behaviours, $EuGdCuS_3$ is classified as an L-type ferrimagnet [8].

Around the transition temperature, the χ–T and M–H curves of $EuGdCuS_3$ show ferrimagnetic behaviour. According to molecular field theory, the temperature dependence of the reciprocal magnetic susceptibility for ferrimagnets is represented by [8]

$$\frac{1}{\chi - \chi_{TIP}} = \frac{T}{C} + \frac{1}{\chi_0} - \frac{\sigma}{T - \Theta}, \tag{4}$$

where χ_0, Θ, σ are parameters related to the molecular field coefficients. The Curie temperature T_C ($=(\Theta - C/\chi_0 + \sqrt{(\Theta - C/\chi_0)^2 + 4C(\Theta/\chi_0 + \sigma)})/2$) and the Curie constant C ($=C_{Gd} + C_{Eu}$) of $EuGdCuS_3$ are determined as 5.37(7) K and 15.51(1) emu K mol^{-1}, respectively, by fitting equation (4) to the χ^{-1}–T curve as shown in figure 9(b). This value of T_C agrees with the λ-type anomaly temperature (5.1 K) in the C_{mag}–T curve.

3.2.3. $EuRCuS_3$ (R = Tb, Dy, Tm). For the $EuRCuS_3$ compounds with R = Tb, Dy, and Tm, the χ–T curves and M–H curves are similar. Figure 12(a) shows the temperature

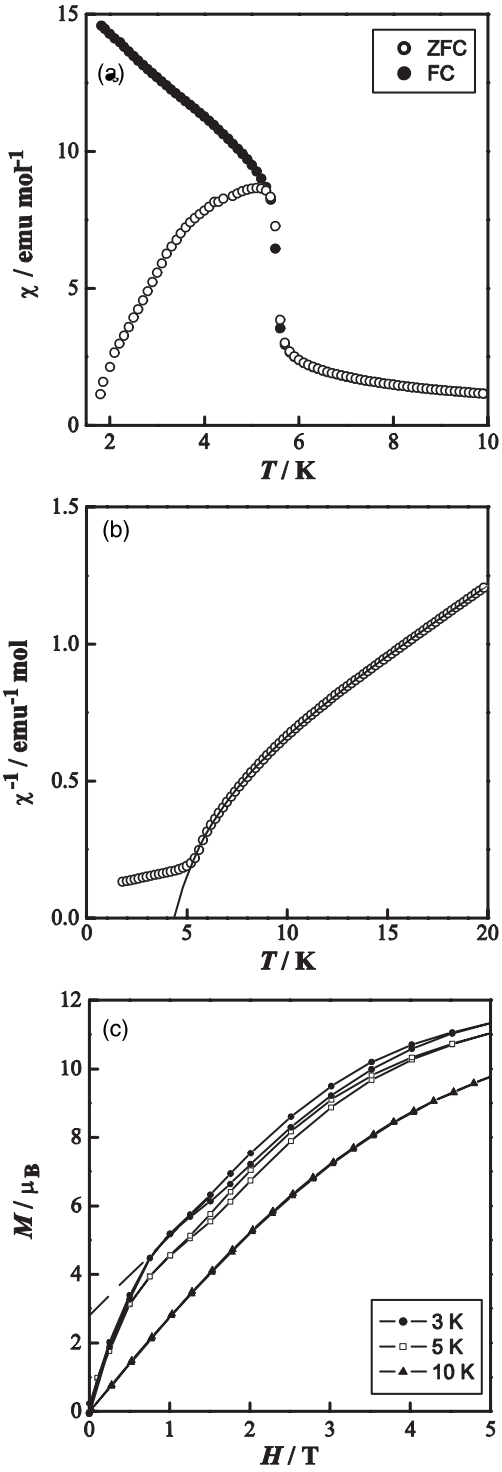

Figure 12. (a) The temperature dependence of the magnetic susceptibility (χ) for $EuTbCuS_3$ below 10 K. (b) The temperature dependence of the reciprocal magnetic susceptibility (χ^{-1}) for $EuTbCuS_3$ below 20 K. A solid curve is the result of fitting with the molecular field approximation. (c) The field dependence of the magnetization for $EuTbCuS_3$.

Table 3. Magnetic properties of $EuRCuS_3$.

R	T_C (K)	C(obs) (emu K mol^{-1})	C(calc) (emu K mol^{-1})
Gd	5.4	15.51(1)	15.77
Tb	4.9	18.34(1)	19.70
Dy	4.6	21.53(1)	22.07
Tm	4.8	14.44(1)	15.03

dependence of the magnetic susceptibilities of $EuTbCuS_3$. A divergence between the ZFC and FC susceptibilities, which is due to a ferrimagnetic ordering, is observed at 5.4 K for $EuTbCuS_3$. Other $EuRCuS_3$ (R = Dy, Tm) compounds also show a ferrimagnetic transition at 5.3 K for $EuDyCuS_3$ and at 5.4 K for $EuTmCuS_3$. T_C and C ($=C_R + C_{Eu}$) for $EuRCuS_3$ (R = Tb, Dy, Tm) were determined by fitting equation (4) to the χ^{-1}–T curve. The fitting result for $EuTbCuS_3$ is shown in figure 12(b), and the parameters fitted for $EuRCuS_3$ (R = Tb, Dy, Tm) are listed in table 3 together with the data for $EuGdCuS_3$. The value of C is smaller than the sum of the Curie constants for free R^{3+} ($^7F_6$ for Tb^{3+}, $^6H_{15/2}$ for Dy^{3+}, $^3H_6$ for Tm^{3+}) and Eu^{2+} ($^8S_{7/2}$) ions, which indicates that the crystal electric field affects the R^{3+} ions. Figure 12(c) shows the field dependence of the magnetization for $EuTbCuS_3$. The M–H curves at 3 and 5 K demonstrate ferrimagnetic behaviour, while that at 10 K shows paramagnetic behaviour. The value of magnetization $\sim$11 μ_B at 5 T in the M–H curve at 3 K is considerably smaller than the theoretical moment for the free Eu^{2+} and Tb^{3+} ions ($gS + g_J J = (7 + 9)\ \mu_B = 16\ \mu_B$). Because the crystal electric field does not affect the Eu^{2+} ions, this large reduction of the magnetic moment should be mainly attributable to the crystal field effect on the Tb^{3+} ions. Assuming that the magnetic moment of the Tb^{3+} ground state is equal to $\sim$4 μ_B and that these Tb^{3+} moments form a ferromagnetic net, the ferrimagnetic state with the antiferromagnetic coupling of the Tb^{3+} and Eu^{2+} ferromagnetic nets is expected to have the remanent magnetization of $\sim$3 μ_B and the magnetization should saturate, reaching $\sim$11 μ_B with increasing applied magnetic field. The M–H curve at 3 K indicates that the saturation moment of the field-induced ferrimagnetic state can be estimated to be 2.9 μ_B by extrapolation of the magnetic moment between 0.8 and 1.5 T to zero field (a broken curve in figure 12(c)). This result supports the assumption that the Tb^{3+} ground state has the magnetic moment of $\sim$4 μ_B and forms a ferromagnetic net.

3.2.4. $EuYbCuS_3$. Figures 13(a) and (b) show the χ–T and M–H curves of $EuYbCuS_3$, respectively. The behaviour is seen to be ferromagnetic at a glance. A divergence between the ZFC and FC susceptibilities is observed at 5.5 K. From the Curie–Weiss fitting using equation (1) to the χ–T curve above 100 K, the Curie constant is estimated to be 8.80 emu K mol^{-1}. This value is considerably smaller than the theoretical one (10.41 emu K mol^{-1}). It is considered that Yb^{3+} is strongly affected by the crystal field. The ground $^2F_{7/2}$ state of the Yb^{3+} ions should be split into four Kramers doublets under the D_{2h} point symmetry in $EuYbCuS_3$ and the low lying Kramers doublet of the Yb^{3+} moments should show magnetic ordering. It is suggested that the ferromagnetic behaviour of the $^8S_{7/2}$ moment of Eu^{2+} conceals the magnetic ordering of the small Yb^{3+} magnetic moment.

4. Summary

Novel quaternary rare-earth copper sulfides $EuRCuS_3$ (R = Y, Gd–Lu) have been synthesized. These compounds crystallize in the Eu_2CuS_3-type structure for R = Y, Gd–Dy and in

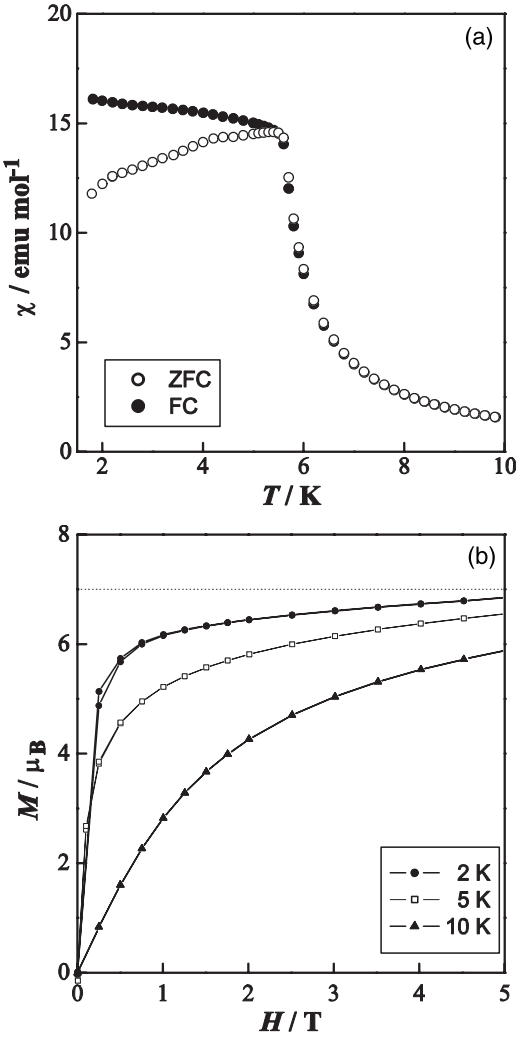

Figure 13. (a) The temperature dependence of the magnetic susceptibility (χ) for $EuYbCuS_3$ below 10 K. (b) The field dependence of the magnetization for $EuYbCuS_3$.

the $KZrCuS_3$-type structure for R = Tm–Lu. Both $EuYCuS_3$ and $EuLuCuS_3$ show a ferromagnetic ordering of the Eu^{2+} ion at around 5.0 K. The other $EuRCuS_3$ compounds containing magnetic R ions show a ferrimagnetic transition at around 5.0 K.

References

[1] Mitchell K and Ibers J A 2002 *Chem. Rev.* **102** 1929
[2] Lemoine P, Carre D and Guittard M 1986 *Acta Crystallogr.* C **42** 390
[3] Furuuchi F, Wakeshima M and Hinatsu Y 2004 *J. Solid State Chem.* at press
[4] Izumi F and Ikeda T 2000 *Mater. Sci. Forum* **321–324** 198–203
[5] Christuk A E, Wu P and Ibers J A 1994 *J. Solid State Chem.* **110** 330
[6] Wu P, Christuk A E and Ibers J A 1994 *J. Solid State Chem.* **110** 337
[7] Yang Y and Ibers J A 1999 *J. Solid State Chem.* **147** 366
[8] Néel L 1948 *Ann. Phys.* **3** 137